Journal of Inflammation Research

Dovepress
Taylor & Francis Group

Open Access Full Text Article

ORIGINAL RESEARCH

Rhein Mitigates Lung Injury in Severe Acute Pancreatitis Through the Inhibition of MARK4-Mediated Microtubule Destabilization

Zhenxuan Sun[1–3,*], Jie Liu[1–3,*], Peng Ge[1–3,*], Yinan Cao[4], Jin Liu[1–3], Haiyun Wen[1–3], Xinyu Luo[1–3], Boliang Pei[1–3], Zuocang Jin[1,3], Huijuan Li[3], Lu Xun[1–3], Yalan Luo[5], Qi Yang[6], Hailong Chen[1–3]

[1]Department of General Surgery, The First Affiliated Hospital of Dalian Medical University, Dalian, Liaoning, 116011, People's Republic of China; [2]Institute (College) of Integrative Medicine, Dalian Medical University, Dalian, Liaoning, 116011, People's Republic of China; [3]Laboratory of Integrative Medicine, The First Affiliated Hospital of Dalian Medical University, Dalian, Liaoning, 116011, People's Republic of China; [4]Day Surgery Center, Dalian Municipal Central Hospital, Dalian, Liaoning, 116033, People's Republic of China; [5]Department of Gastroenterology, The First Affiliated Hospital of Dalian Medical University, Dalian, Liaoning, 116011, People's Republic of China; [6]Department of Traditional Chinese Medicine, The Second Affiliated Hospital of Dalian Medical University, Dalian, Liaoning, 116023, People's Republic of China

*These authors contributed equally to this work

Correspondence: Hailong Chen, Department of General Surgery, The First Affiliated Hospital of Dalian Medical University, Zhongshan Road 222, Dalian, Liaoning, 116011, People's Republic of China, Tel +86 411 83635963, Fax +86 411 83622844, Email chenhailong@dmu.edu.cn

Purpose: Explore the therapeutic effect and molecular mechanism of rhein on severe acute pancreatitis associated acute lung injury (SAP-ALI).

Methods: The SAP-ALI rat model was constructed by retrograde injection of 5% sodium taurocholate into the pancreaticobiliary duct, and pulmonary microvascular endothelial cell (PMVEC) injury model was induced by LPS. The potential therapeutic effects and appropriate dosages of rhein on SAP-ALI and PMVEC were investigated in both in vivo and in vitro experiments. Furthermore, the regulatory role of MARK4 in the related pathological process were confirmed by some experimental methods. RNA sequencing analysis was performed to explore the potential downstream genes of MARK4. Moreover, the regulatory effect of rhein on MARK4 was validated through molecular docking and rescue experiments.

Results: Rhein intervention had potential therapeutic effects on acute lung injury triggered by SAP and pulmonary endothelial cell injury induced by LPS. MARK4 may contribute to pulmonary endothelial cell injury through the modulation of microtubule structure. Compared with LPS stimulation, a total of 2081 differentially expressed genes were identified after MARK4 knockdown. The results of molecular docking and rescue experiments indicated that rhein may exert its protective effects by targeting MARK4.

Conclusion: Rhein may regulate the microtubule structure by targeting MARK4, thereby alleviating SAP-ALI and LPS-induced pulmonary endothelial cell injury.

Keywords: rhein, microtubule, severe acute pancreatitis, acute lung injury

Introduction

Acute pancreatitis (AP) is one of the common diseases encountered in general surgical clinical practice, with approximately 15% to 20% of patients experiencing a deterioration of their condition, developing into severe acute pancreatitis (SAP). The mortality rate for these patients can be as high as 20%.[1] When SAP further deteriorates, localized pancreatic inflammation may evolve into systemic inflammatory response syndrome (SIRS), accompanied by organ dysfunction, and can even progress to multiple organ dysfunction syndrome (MODS), which may ultimately lead to death. Among SAP patients, the most common and earliest organ dysfunction is lung injury. According to statistics, about 45% of SAP patients suffer from acute lung injury (ALI), clinically manifested as acute respiratory distress syndrome (ARDS).[2] Therefore, the prevention and early intervention of lung injury are vital measures to reduce the mortality rate of SAP

Received: 6 November 2024
Accepted: 19 January 2025
Published: 30 January 2025

patients. Despite in-depth research and exploration into the pathogenesis of ALI caused by SAP in recent years, many pathophysiological mechanisms remain to be elucidated.

The endothelial barrier constructed by pulmonary microvascular endothelial cells plays a crucial role in maintaining the integrity of the air-blood barrier structure. An intact endothelial barrier can effectively prevent the infiltration of water, red blood cells, inflammatory factors, and immune cells into the pulmonary interstitium, thereby effectively curbing the onset of lung inflammation and the progression of functional impairment.[3,4] However, in the case of acute lung injury, the permeability of the pulmonary endothelial barrier significantly increases, leading to substantial leakage of intravascular fluid and inflammatory mediators, which not only exacerbates pulmonary edema but also further promotes the deterioration of inflammation.[5]

Microtubules (MT) are essential components of the cytoskeleton and play a vital role in maintaining cell shape, performing cellular functions, and facilitating intercellular connections in critical biological activities.[6] During lung injury induced by oxidative stress, the excessive production of reactive oxygen species (ROS) leads to the depolymerization of microtubules, which subsequently triggers a dysfunction of the endothelial barrier.[7] Danielle B Buglak et al have discovered that under pathological conditions, the microtubule skeleton within pulmonary endothelial cells undergoes depolymerization. This process disrupts the intercellular VE-cadherin connections and consequently leads to alterations in the structure of the endothelial barrier.[8] These research findings suggest that microtubules may play a pivotal role in the pathological mechanism of endothelial barrier dysfunction in severe acute pancreatitis-associated acute lung injury (SAP-ALI), making microtubules a potential therapeutic target for SAP-ALI. However, the specific mechanism of MT regulation during endothelial injury is still not precise. This study hypothesizes that microtubule affinity-regulating kinase 4 (MARK4) may be crucial in this process.

Rhein, one of the main active components in rhubarb, belongs to the anthraquinone compound family. It possesses significant anti-inflammatory and anti-tumor properties.[9,10] In treating various diseases such as chronic glomerulonephritis,[11] cardiac hypertrophy,[12] obesity,[13] and Parkinson's disease,[14] rhein has demonstrated its efficacy. In sepsis or LPS-induced mouse models, rhein can mitigate corresponding lung injury by regulating the overactivation of macrophages and targeting the regulation of specific genes.[15,16] Additionally, in mouse models infected with respiratory syncytial virus, rhein has been proven to effectively improve lung injury conditions by inhibiting inflammasome activation.[17]

This study aims to delve into the dynamic changes of the microtubule cytoskeleton within pulmonary microvascular endothelial cells during the process of SAP-ALI, as well as the regulatory role of MARK4 in this pathological process. Additionally, this research will explore how rhein exerts its therapeutic effects on SAP-ALI through its pharmacological mechanisms, to provide new insights and strategies for revealing the pathogenesis and precision treatment of SAP-ALI.

Materials and Methods

Reagents and Antibodies

Rhein (HY-N0105) and MARK4 inhibitor PCC0208017 (#HY-139604) were purchased from Med Chem Express (New Jersey, USA). Lipopolysaccharide (LPS, #tlrl-pb5lps) was purchased from InvivoGen (Toulouse, France). Tumor necrosis factor-alpha (TNF-α, #F16960), interleukin-6 (IL-6, #F15870), and interleukin-1beta (IL-1β, #F15810) kits were purchased from Westang Biotechnology (Shanghai, China). Aspartate aminotransferase (AST, #C010-2-1), alanine aminotransferase (ALT, #C009-2-1), alkaline phosphatase (AKP, #A059-2-2), blood urea nitrogen (BUN, #C013-2-1), creatinine (CREA, #C011-2-1) and amylase (#C016-1-1) kits were purchased from Nanjing Jiancheng Bioengineering Institute (Nanjing, China).

MARK4 rabbit antibody (#4834; 1:1000) for WB was purchased from Cell Signaling Technology (Boston, USA). VE-cadherin rabbit antibody (#36-1900; 1:200) was purchased from Thermo Fisher Scientific (Waltham, USA). MARK4 rabbit antibody (#20174-1-AP; 1:200) for IF, MAP4 rabbit antibody (#11229-1-AP; 1:1000), PIEZO1 rabbit antibody (#15939-1-AP; 1:800), α-tubulin mouse antibody (#66031-1-Ig; 1:500) for IF, 594-goat anti-rabbit recombinant secondary antibody (#RGAR004; 1:200), and 488-goat anti-mouse recombinant secondary antibody (#RGAM002; 1:200) were purchased from Proteintech (Rosemont, USA). MAP4 phosphor S1073 rabbit antibody (#PAB15916, 1:1000) was purchased from Abnova (China). Acetyl-alpha Tubulin rabbit antibody (#AF4351, 1:1000), α-tubulin rabbit antibody (#AF7010; 1:10000), and goat

anti-rabbit secondary antibody (#S0001; 1:8000) were purchased from Affinity Biosciences (Liyang, China), GAPDH rabbit antibody (#AC001; 1:20000) was purchased from ABclonal Technology (Wuhan, China).

Animals and Experiments

Male Sprague-Dawley rats (180–220g) were obtained from the Experimental Animal Center of Dalian Medical University. All rats were housed in a pathogen-free circumstance with a 12h light-dark cycle, 55±5% humidity and 22 ±2°C, allowed free standard rodent chow and water. All rats were adaptively fed for one week before experimental procedures. All animal experiments were approved by the Committee for Research and Animal Ethics of Dalian Medical University and were in accordance with the Guidelines for the Care and Use of Laboratory Animals developed by the National Institutes of Health, USA. To ascertain the safe dosage range and potential toxicity threshold of rhein, we thoroughly assessed its effects on liver and kidney function in rats across various dosages. Firstly, 36 rats were randomly divided into six groups: the control group (CON), the 50 mg/kg rhein treatment group (50mg/kg), the 100 mg/kg rhein treatment group (100mg/kg), the 150 mg/kg rhein treatment group (150mg/kg), the 200 mg/kg rhein treatment group (200mg/kg), and the 250 mg/kg rhein treatment group (250mg/kg). Rats in the rhein treatment groups received gavage administration of respective concentration rhein at 0 hours, followed by a second administration of the same dose at 12 hours. The CON group was administered an equivalent volume of 0.9% sterile saline by gavage at 0 and 12 hours. All rats were sacrificed at 24 hours, and blood samples were collected from the abdominal aorta, along with liver and kidney tissues for further analysis. Then, 50 rats were randomly divided into five groups: sham operation group (SO), SAP group (SAP), SAP+50mg/kg rhein group (SAP+50), SAP+100mg/kg rhein group (SAP+100), and SAP+150mg/kg rhein group (SAP+150). The SAP rat models were constructed following a previously established method:[18] retrograde injection of 5% sodium taurocholate (50 mg/kg, 0.1 mL/min) into the rat pancreaticobiliary duct. The SO group rats received an equivalent volume of 0.9% sterile saline via retrograde injection into the pancreaticobiliary duct. The rhein treatment groups were administered with rhein at doses of 50 mg/kg, 100 mg/kg, and 150 mg/kg by gavage immediately after SAP modeling and again at 12 hours post-modeling. All rats were sacrificed 24 hours after the modeling. Bronchoalveolar lavage fluid (BALF) and blood from the abdominal aorta, pancreas, and lung tissues were collected for further analysis. Finally, 40 rats were randomly divided into four groups: sham operation group (SO), SAP group, SAP+PCC0208017 group (SAP+PCC), and SAP+150mg/kg rhein group (SAP+150). The SO group, SAP group, and SAP+150 group were constructed as described above, while the SAP+PCC group was given PCC0208017 (50mg/kg) by gavage immediately after SAP modeling. All rats were sacrificed 24 hours after modeling. BALF, blood from the abdominal aorta, and lung tissues were collected for further analysis.

Cell Culture and Experimental Design

Rat pulmonary microvascular endothelial cells (R-PMVECs, #PC-150r) were purchased from SAIOS Biology (Wuhan, China). Rat endothelial cell growth supplement (ECGS-r, #1062) was purchased from ScienCell (San Diego, USA). DMEM medium (#11965092) and fetal bovine serum (#A5670701) were purchased from GIBCO Thermo Fisher Scientific (Waltham, USA). R-PMVECs were cultured in DMEM with 20% fetal bovine serum and 1% rat endothelial cell growth supplement in the incubator at 5% CO_2, 37°C.

Firstly, R-PMVECs were divided into five groups: the control group (CON), the LPS group (LPS), the LPS+5μM rhein group (LPS+5), the LPS+20μM rhein group (LPS+20), and the LPS+40μM rhein group (LPS+40). R-PMVECs were seeded into 6-well plates. The CON group cells were cultured in a normal medium without any treatment, the LPS group cells were stimulated with 100 ng/mL LPS for 24 hours, and the cells of the other three groups were treated with corresponding doses of rhein for 24 hours after 24 hours of LPS stimulation. Cells and supernatants were collected for further analysis. Then, R-PMVECs were divided into four groups: the control group (CON), the LPS group (LPS), the LPS+sh-NC group (LPS+sh-NC), and the LPS+sh-MARK4 group (LPS+sh-MARK4). The treatment of CON and LPS groups was the same as above. The cells of LPS+sh-NC and LPS+sh-MARK4 groups were transfected with negative control or MARK4-knockdown plasmids and stimulated with LPS for 24 hours. Cells and supernatants were collected for further analysis. Finally, R-PMVECs were divided into five groups: the control group (CON), the LPS group (LPS), the LPS+40μM rhein group (LPS+40), the LPS+40μM rhein +oe-NC group (LPS+40+oe-NC), and the LPS+40μM rhein

+oe-MARK4 group (LPS+40+oe-MARK4). The treatment of CON, LPS, and LPS+40 groups was the same as above. The cells of LPS+40+oe-NC and LPS+40+oe-MARK4 groups were transfected with negative control or MARK4-overexpression plasmids after LPS and rhein treatments. Cells and supernatants were collected for further analysis.

Histological Examination

5% sodium taurocholate had the most direct and immediate effect on pancreatic head tissue, causing more substantial pathological alterations. As a result, we conducted histological examinations of rats' pancreatic head areas. The tissue samples were first fixed in 4% paraformaldehyde. After embedded in paraffin, samples were cut into 5μm sections. After undergoing dewaxing and dehydration procedures, tissue sections were stained with hematoxylin-eosin (HE) and subjected to pathological examination under an optical microscope. The pathological scoring criteria for the pancreas and lungs were shown in Supplementary Tables 1 and 2.

Measurement of Serum ALT, AST, AKP, BUN, CREA and Amylase

Blood was obtained from the abdominal aorta of rats, spun at 3000 rpm at 4°C for 10 min, and serum was isolated. Per the kit's instructions, the absorbance of standard well, assay well, and blank well was measured using a multifunctional microplate reader, and the concentrations of serum ALT, AST, AKP, BUN, CREA, and amylase were determined.

Enzyme-Linked Immunosorbent Assay (ELISA)

The concentrations of TNF-α, IL-6, and IL-1β in serum and cell supernatant were detected by corresponding ELISA kits.

Extraction of Tubulin Fraction

The polymeric tubulin and monomeric tubulin were extracted using the previous study method.[19] Briefly, the samples were first washed twice with microtubule stabilizing solution (MTSB) at 37°C. MTSB contained 0.1M piperazine-N, N ′-bis (2-ethylsulfonic acid) (PIPES, #P8320), 2mM ethylene glycol bis (2-aminoethyl ether) - N, N, N′, N ′- tetraacetic acid (EGTA, #E8050), 0.1mM Ethylenediaminetetraacetic acid (EDTA, #E8040), and 0.5mM MgCl2 (#IM9032). Then, MBST+0.1% Triton X-100 (# T8200) was used to incubate the sample (37°C) with 20% glycerol (pH6.8, #G8190) to separate polymerized and non-polymerized microtubule (ie monomeric microtubule) for the Western Blot analysis. The above reagents were purchased from Beijing Solarbio Science & Technology (Beijing, China).

Western Blot Analysis

Protein from rats and cells was extracted and quantified using a protein extraction kit (KGB5303-100, KeyGEN BioTECH, Nanjing, China) and a BCA protein assay kit (#KGB2101-500, KeyGEN BioTECH, Nanjing, China). Multicolor prestained protein ladder marker (#WJ103) was purchased from Epizyme Biotech (Shanghai, China). The equivalent amounts of protein samples were separated by SDS-polyacrylamide gel electrophoresis (6–10%) and then transferred onto polyvinylidene fluoride (PVDF) membranes. The membranes were blocked with 5% skim milk, followed by incubation with the appropriate primary antibody at 4°C overnight. After washing with Tris-buffered saline Tween 20 (TBST), the membranes were incubated with the secondary antibody for 1 hour. Finally, the protein bands were detected using the chemiluminescence system (Tanon-5200, Shanghai, China) for exposure. ImageJ software was used to statistically analyze band intensities normalized to GAPDH. We used the "Measure" function to get the average gray value for the area corresponding to each protein band. All measured gray values were exported and documented. GAPDH was designated as the internal reference; the gray value of each target band was divided by the corresponding gray value of the internal reference to get the normalized relative expression. The normalized data were subjected to statistical analysis.

Quantitative Real-Time PCR

Total RNA from rats and cells was extracted using a total RNA extraction kit (#M5101, New Cell Molecular Biotech, Suzhou, China). 1μg RNA of each sample was transcribed reversely into cDNA using All-in-One First-Strand Synthesis MasterMix (#EG15133S, Yugong Biotech, Lianyungang, China). For amplification, synthetic cDNA was amplified by

Taq SYBR® Green qPCR Premix (#EG20117M, Yugong Biotech, Lianyungang, China). PCR conditions were initial denaturation at 95°C for 30s, 40 cycles of denaturation at 95°C for 10s, annealing, and extension at 64°C for 30s. The data were analyzed using the $2^{-\Delta\Delta CT}$ method, and all results were adjusted to the GAPDH level. All primer sequences were shown in Supplementary Table 3.

Measurement of Lung Wet/Dry Weight (W/D) Ratio

Fresh right lungs (upper lobe) of each group of rats were removed, dried with filter paper, weighed and recorded for weight, and dried at 65°C for 48 hours before being weighed again and recorded. Then, the wet/dry weight ratio was calculated for further analysis.

Quantification of Protein in BALF

The tracheae of each group of rats were fully exposed during the sampling process. After ligating the right main bronchus, 5 mL of 0.9% sterile saline was instilled into the trachea through a small incision using a lavage needle. After 1 minute, BALF from the left lung was collected, and this procedure was repeated 3 times. The collected BALF was centrifuged (4°C, 3000 rpm, 10 minutes), and the supernatant was then taken to measure the protein concentration using a BCA protein assay kit.

Assessment of Lung Vascular Leakage

Evans blue dye (#E6135, MACKLIN, Shanghai, China) was injected into the tail vein of rats (30mg/kg) 2 hours before modeling. Then freshly isolated lung tissues were treated with formamide (#F6287, MACKLIN, Shanghai, China) in a 37°C water bath for 48 hours, centrifuged at 1000 g, 4°C for 10 minutes, and finally, the concentration of Evans blue dye in the supernatant was detected at 620nm to represent lung leakage.

Transfection

Four rat MARK4 RNA knockdown sequences, one rat MARK4 overexpression sequence, and two corresponding negative control sequences were designed and assembled into short hairpin RNAs (sh-MARK4, sh-NC, oe-MARK4, oe-NC) by GenePharma (Suzhou, China), the sequences were shown in Supplementary Table 4. Cells were transfected using Lipofectamine™ 2000 Transfection Reagent (#11668500, Invitrogen, Carlsbad, USA) according to the instructions provided.

Cell Viability Assay

The Cell Counting Kit-8 (CCK-8, #K1018, APExBIO, Huston, USA) was used to evaluate the effect of different doses of rhein on R-PMVEC activity. R-PMVECs were seeded into 96-well microplates in a culture medium and incubated for 24 h. Then, the cells were treated with the different concentrations of rhein (0, 5, 10, 20, 40, 60, 80, or 100 μM) for 24 h in 5% CO2 at 37°C. After this, 10 μL of CCK-8 reagent was added per well, and the plates were incubated for 2 h in darkness at 37 °C, and absorbance at 450 nm was measured with a microplate reader (BioTek, Winooski, USA).

Immunofluorescence

5μm thick rat lung paraffin-embedded sections were dewaxed and hydrated, followed by antigen retrieval and blocking. The sections were incubated overnight at 4°C with a mixture of MARK4 primary antibody and α-tubulin primary antibody and then incubated for 1 hour at 37°C with the corresponding mix of two secondary antibodies. Finally, the cell nuclei were stained with DAPI (#C0065, Beijing Solarbio Science & Technology, Beijing, China) at room temperature. R-PMVEC were seeded on confocal dishes, fixed with 4% paraformaldehyde at room temperature for 15 minutes, permeabilized with 0.1% Triton-X-100 at room temperature for 15 minutes, and blocked for 1 hour at room temperature before incubation overnight at 4°C with the same mixture of MARK4 primary antibody and α-tubulin primary antibody. The corresponding two secondary antibodies were then incubated for 1 hour at 4°C. Finally, the cell nuclei were stained with DAPI at room temperature.

RNA Sequencing

First, the purity of the extracted RNA samples was tested, with the criteria being 1.8 < OD260/280 < 2.0 and OD260/230 ≥ 2.0. Then, the RNA libraries were subjected to quality control and sequencing by Novogene (Beijing, China), and sequencing data analysis was performed using the NovoMagic platform (https://magic-plus.novogene.com).

Molecular Docking

The 3D structure of MARK4 was obtained from the RCSB PDB database (5ES1, https://www.rcsb.org), and the 3D structure of rhein was obtained from the PubChem database (https://pubchem.ncbi.nlm.nih.gov). Molecular docking was performed using AutoDock Vina 1.1.2,[20,21] and a binding energy of less than −5 kJ/mol indicated strong affinity. The 3D structure of the MARK4 and rhein complex was visualized using PyMOL 2.2.0.

Statistical Analysis

Statistical analysis was conducted utilizing R (4.3.1) software. Data exhibiting normal distribution and homogeneous variance were represented as mean ± SD. Multiple comparisons were executed via one-way ANOVA, with the LSD *t*-test employed as a post-hoc analysis. The median with interquartile range was utilized for data characterized by non-normal distribution or heterogeneous variance. The Kruskal–Wallis test facilitated multiple comparisons, and the Dunn or Mann–Whitney *U*-test was applied for pairwise comparisons. A P-value of less than 0.05 denoted a statistically significant difference.

Results

Rhein Ameliorated R-PMVEC Injury

We first conducted a CCK8 toxicity experiment of rhein on normal R-PMVEC (Figure 1A). The low (5μM, LPS+5), medium (20μM, LPS+20), and high (40μM, LPS+40) concentrations were selected as the intervention doses of rhein after LPS stimulation in subsequent experiments. The rhein can ameliorate LPS-induced R-PMVEC inflammation, and this therapeutic effect was concentration-dependent (Figure 1B–D). Thus, 40μM was chosen as the rhein administration concentration for subsequent in vitro experiments. Additionally, the protein expression levels of VE-cadherin, acetyl-alpha tubulin, and polymeric tubulin in the LPS group were significantly lower than those in the CON group (Figure 1E). In contrast, the protein expression level of monomeric tubulin was increased considerably. After rhein intervention, the changes above were relieved to varying degrees, indicating that rhein can ameliorate the injury of the endothelial barrier and microtubules caused by LPS in R-PMVEC.

The Effects of Different Doses of Rhein on Liver and Kidney Function in Rats

Compared with the CON group, the liver histopathology sections of the 50 mg/kg, 100 mg/kg, and 150 mg/kg groups (Figure 2A) revealed no signs of hepatocyte damage, necrosis, or immune cell infiltration, with the liver lobule structure remaining intact. Common liver function markers, such as ALT, AST, and AKP, showed no statistically significant differences from the CON group (Figure 2C–E). However, the 200 mg/kg and 250 mg/kg groups exhibited changes in liver pathology, along with statistically significant alterations in liver function markers. In addition, when the dose of rhein reached 200 mg/kg and 250 mg/kg, kidney histopathology sections showed edema, necrosis, and immune cell infiltration (Figure 2B), and the two renal function indicators (Figure 2F and G) showed statistically significant. These findings suggested that rhein doses ranging from 0 to 150 mg/kg do not result in appreciable liver and kidney impairment in rats. Liver and kidney toxicity became apparent at 200 mg/kg, with an increasing trend observed with higher doses.

Therapeutic Effect of Rhein on Pancreatic Injury and Inflammation in SAP Rats

Building on the results of our preliminary experiments, we chose 50 mg/kg (SAP+50), 100 mg/kg (SAP+100), and 150 mg/kg (SAP+150) as the low, medium, and high dosages for rhein administration, respectively. The pancreatic histopathology sections of the SO group revealed clear and intact acinar structures, devoid of edema or immune cell infiltration. Conversely, the pancreatic acinar architecture of SAP rats was compromised, with some exhibiting

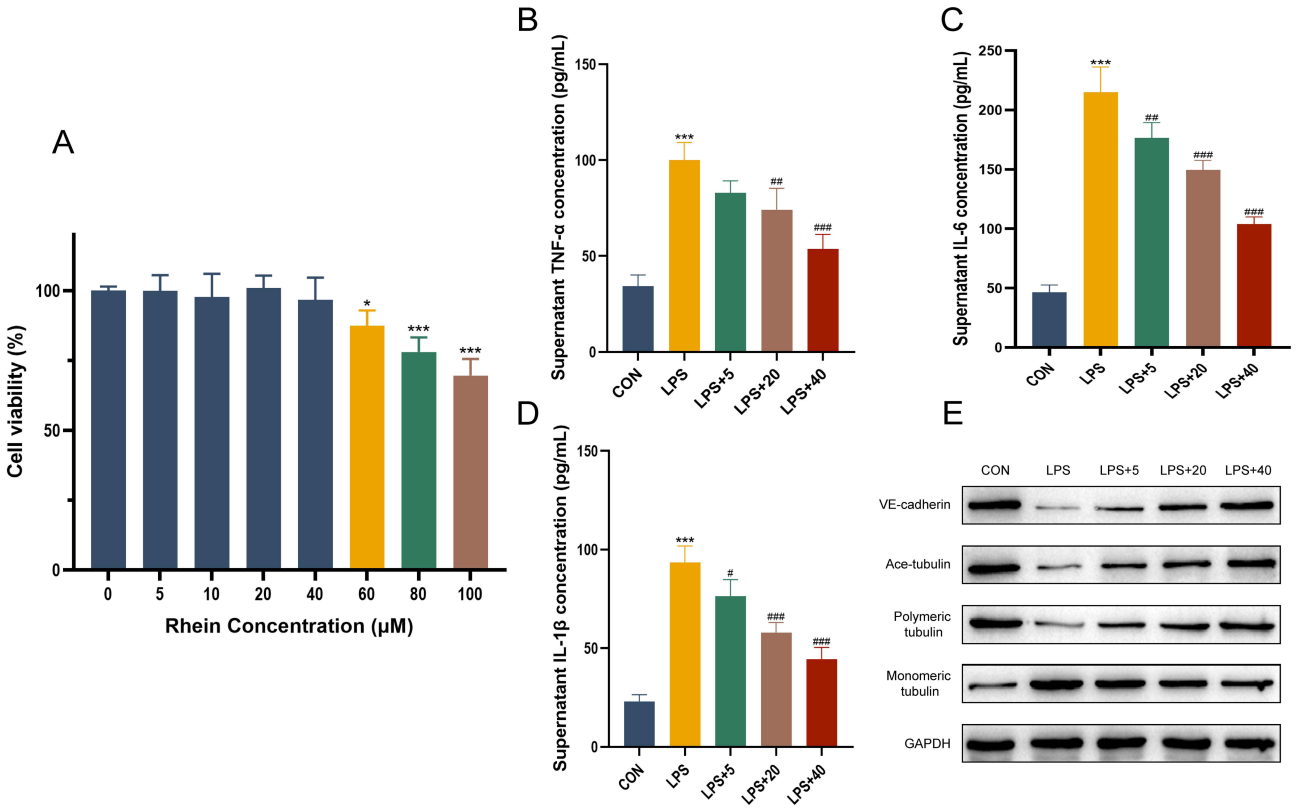

Figure 1 Different doses of rhein ameliorated rat pulmonary microvascular endothelial cell injury. (**A**) Toxicity of different doses of rhein on R-PMVEC was detected by CCK8. (**B–D**) Inflammatory factors TNF-α, IL-6, and IL-1β levels in R-PMVEC culture supernatant were detected by kits separately. (**E**) Protein expression levels of VE-cadherin and MT-related proteins were performed by Western blot. Data were representative images or expressed as mean ± SD of each group at least three independent experiments. ns: no significance; * means P<0.05 compared with CON group; *** means P<0.001 compared with CON group; # means P<0.05 compared with LPS group; ## means P<0.01 compared with LPS group; #### means P<0.001 compared with LPS group.

liquefactive necrosis and concomitant leukocyte infiltration. Pathological sections indicated that three dosages of rhein exhibited varying degrees of reparative effects on pancreatic damage (Figure 3A). Regarding pathological scoring, the 150 mg/kg dosage exhibited the most pronounced decrease in pancreatic damage compared to the SAP group, followed by the 100 mg/kg dosage. No significant difference was seen in the 50 mg/kg group (Figure 3B). Serum amylase is a standard indicator for the early diagnosis of pancreatitis; as depicted in Figure 3C, the SAP group exhibited significantly higher amylase levels than the SO group. Post-treatment with rhein, serum amylase levels decreased notably across all groups. Figure 3D–F illustrated that inflammatory factors were significantly elevated in the SAP group compared to the SO group. Administration of different rhein doses effectively reduced the serum concentrations of inflammatory factors, with the 150 mg/kg dose proving to be the most potent anti-inflammatory efficacy.

Rhein Ameliorated Lung Injury in Rats Induced by SAP

In the SO group, lung histopathology sections revealed a consistent and intact alveolar architecture, devoid of edema, exudation, or immune cell infiltration. Conversely, the SAP group exhibited pronounced alveolar wall thickening, fragmentation, fusion, interstitial hemorrhage, and a marked increase in immune cell infiltration. Rhein administration substantially alleviated these pathological alterations (Figure 4A), with the 150 mg/kg dose showing the most notable treatment effect in lung injury as indicated by pathological scoring (Figure 4B). To evaluate changes in pulmonary vascular permeability, we selected indicators such as the lung wet/dry weight ratio, protein concentration in BALF, and Evans blue dye concentration. The SAP group demonstrated a significant elevation in pulmonary vascular permeability compared to the SO group (Figure 4C–E). However, treatment with rhein, especially at the 150 mg/kg dose, effectively reduced this permeability, leading to the most beneficial outcomes. mRNA expression levels of inflammatory factors

https://doi.org/10.2147/JIR.S505049

https://doi.org/10.2147/JIR.S505049

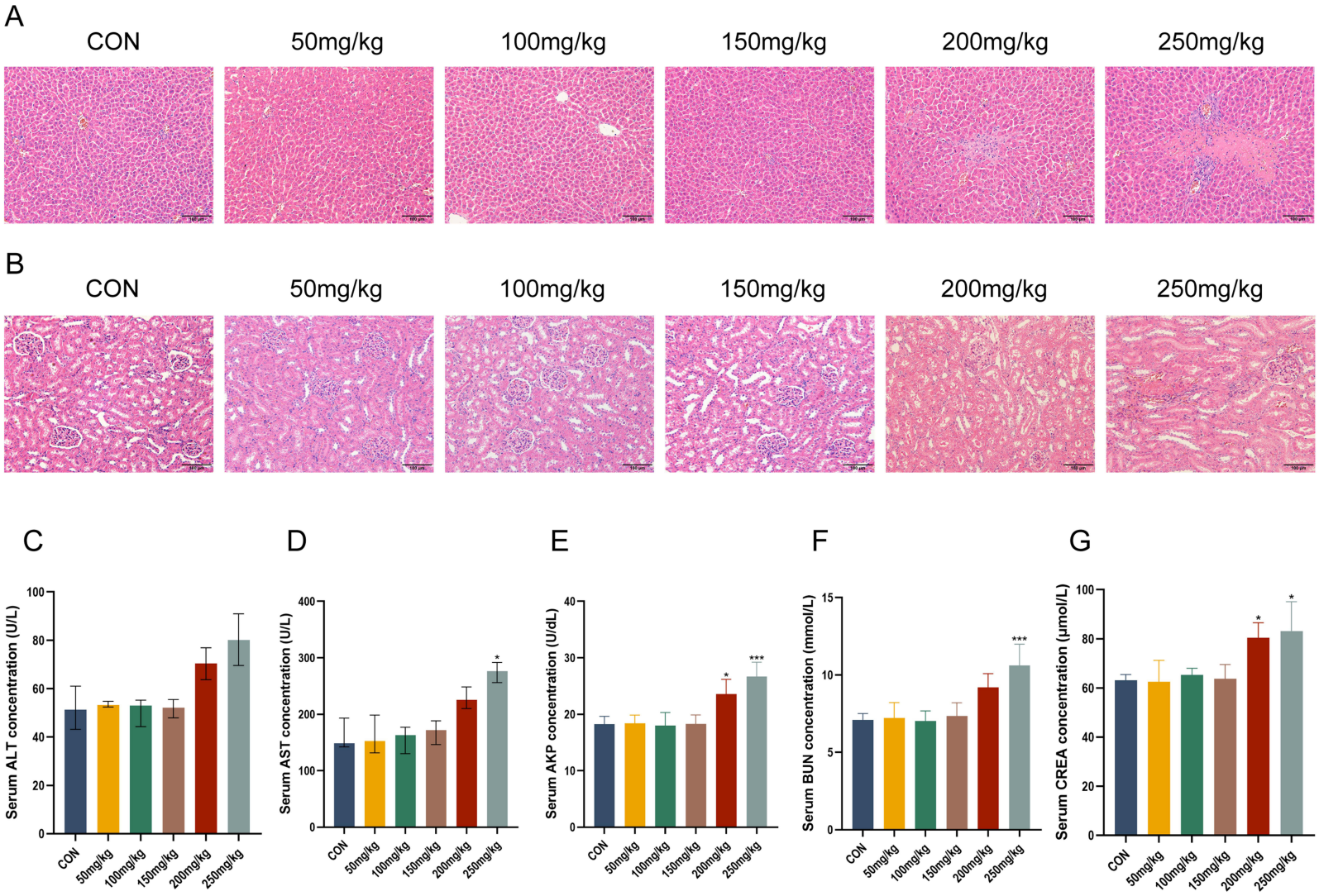

Figure 2 Toxicity of different doses of rhein on the liver and kidney of rats. (**A**) Hematoxylin and eosin (HE) staining was analyzed for pathological changes in rat liver tissues. (**B**) Hematoxylin and eosin (HE) staining was analyzed for pathological changes in rat kidney tissues. (**C–E**) ALT, AST, and AKP levels in rat serum were detected by kits separately. (**F** and **G**) BUN and CREA levels in rat serum were detected by kits separately. Data were representative images or expressed as median with interquartile range (**C** and **D**) or mean ± SD (**E–G**) of each group at least three independent experiments. * means P<0.05 compared with CON group; *** means P<0.001 compared with CON group. scale bar: 100μm.

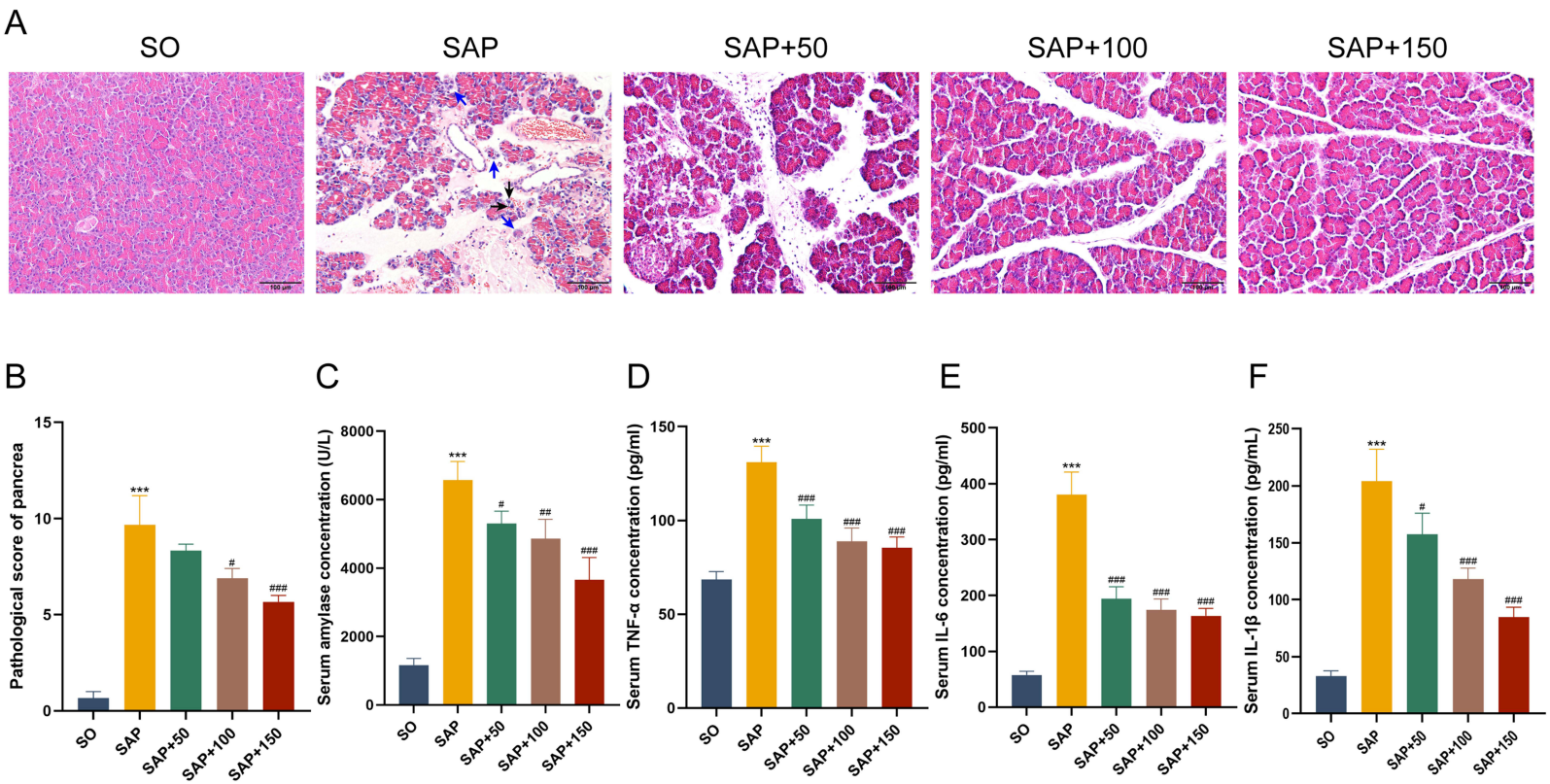

Figure 3 Rhein could ameliorate pancreatic injury and inflammation in SAP rats. (**A**) Hematoxylin and eosin (HE) staining was analyzed for pathological changes in rat pancreatic tissues. Blue arrows: necrosis; Black arrows: inflammatory cells. (**B**) Pathological score of pancreatic tissues in each group. (**C**) Amylase level in rat serum was detected by the kit. (**D**–**F**) TNF-α, IL-6, and IL-1β levels in rat serum were detected by kits separately. Data were representative images or expressed as mean ± SD of each group at least three independent experiments. *** means P<0.001 compared with CON group; # means P<0.05 compared with SAP group; ## means P<0.01 compared with SAP group; #### means P<0.001 compared with SAP group. scale bar: 100μm.

https://doi.org/10.2147/JIR.S505049

https://doi.org/10.2147/JIR.S505049

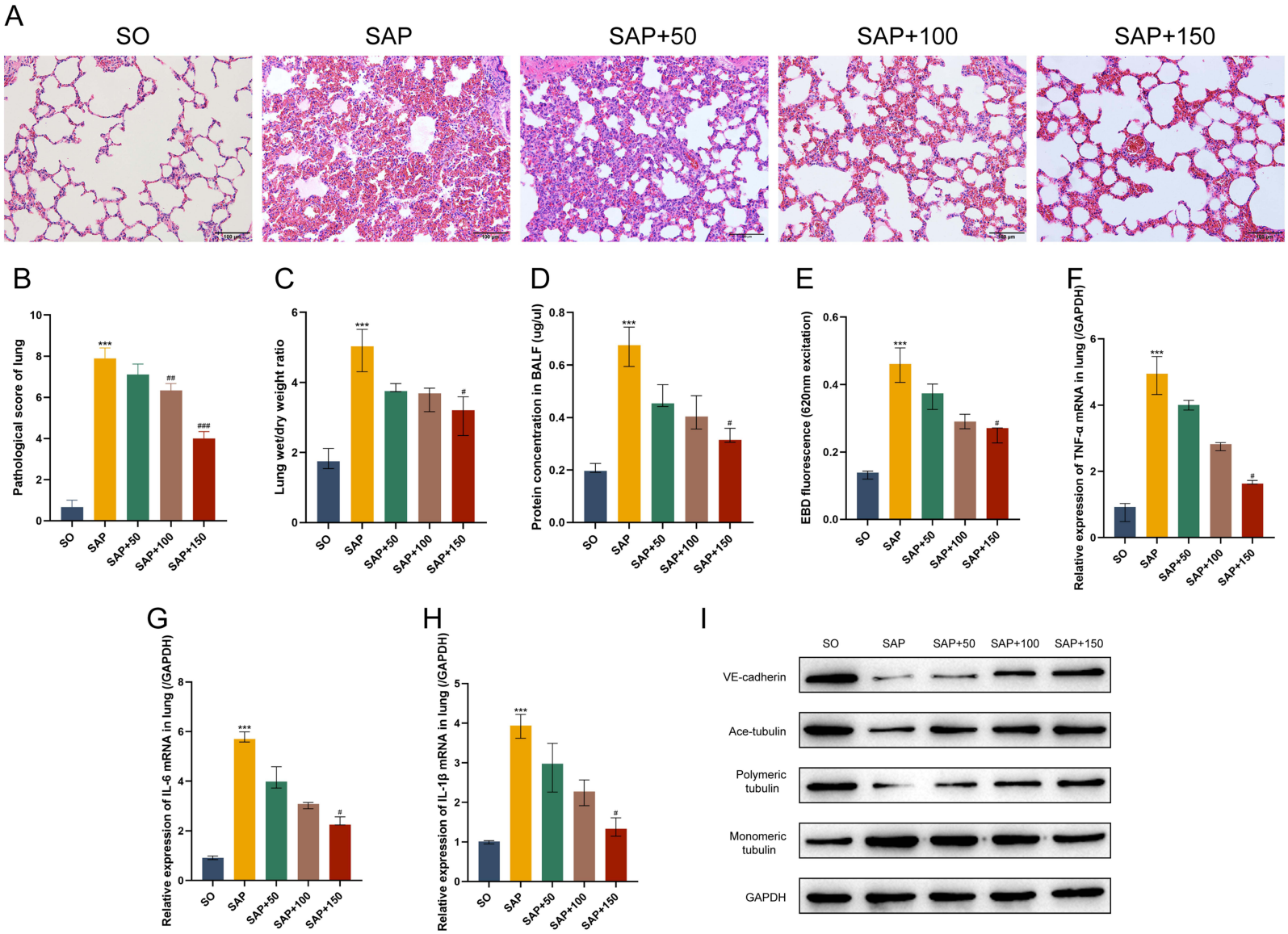

Figure 4 Rhein could ameliorate lung injury in SAP rats. (**A**) Hematoxylin and eosin (HE) staining was analyzed for pathological changes in rat lung tissues. (**B**) Pathological score of lung tissues in each group. (**C–E**) Lung wet/dry weight ratio, protein level, and Evans blue assay in bronchoalveolar lavage fluid reflected pulmonary endothelial barrier function in rats. (**F–H**) TNF-α, IL-6, and IL-1β mRNA relative expressions in rat lungs were performed by Real-Time quantitative PCR. (**I**) Protein expression levels of VE-cadherin and MT-related proteins in rat lungs were performed by Western blot. Data were representative images or expressed as mean ± SD (**B**) or median with interquartile range (**C–H**) of each group at least three independent experiments. *** means P<0.001 compared with CON group; # means P<0.05 compared with SAP group; ## means P<0.01 compared with SAP group; ### means P<0.001 compared with SAP group. scale bar: 100μm.

TNF-α, IL-6, and IL-1β in lung tissues were significantly higher in the SAP group than in the SO group. Rhein treatment dose-dependently decreased these mRNA levels (Figure 4F–H). In SAP rat lung tissues, there was a notable down-regulation of VE-cadherin, acetyl-alpha tubulin, and polymeric tubulin expression, along with a significant upregulation of monomeric tubulin expression, compared to the SO group. Rhein treatment partially reversed these changes (Figure 4I), indicating its potential to repair the destruction of endothelial barrier and MT in the lungs of SAP rats.

Knockdown of MARK4 Ameliorated R-PMVEC Injury

We designed four pairs of RNA interference sequences for MARK4 and conducted screening. RT-qPCR results showed that the expression level of the MARK4 gene was reduced to varying degrees, with the sh-MARK4-2 sequence exhibiting the best knockdown effect. Therefore, this sequence was selected for subsequent experiments (Supplementary Figure 1). Knocking down MARK4 could alleviate the inflammatory response in R-PMVEC after LPS stimulation (Figure 5A–C). LPS stimulation significantly increased the expression level of MARK4 in R-PMVEC compared to the CON group and led to the depolymerization of MT; with the knockdown of MARK4, the levels of p-MAP4 (S1073) and monomeric tubulin significantly decreased, while the levels of polymeric tubulin, acetyl-alpha tubulin, and VE-cadherin partially recovered (Figure 5D–F). These findings suggested that the knockdown of MARK4 in R-PMVEC can reduce inflammation and MT damage induced by LPS.

The Role of MARK4 in R-PMVEC with LPS Stimulation

To further explore the role of MARK4 in the inflammatory response of R-PMVEC, we performed a high-throughput RNA sequencing. PCA findings indicated substantial alterations in the R-PMVEC transcriptome profile after the knockdown of MARK4 expression (Figure 6A). Compared with the LPS group, 2081 differentially expressed genes (DEGs) showed significant changes in the LPS+sh-MARK4 group, with 871 upregulated and 1210 downregulated (Figure 6B and C). Gene Ontology (GO) enrichment analysis showed the DEGs between the LPS+sh-MARK4 group and the LPS group enriched in various biological processes, including cytoskeletal protein binding and Rho GTPase binding (Figure 6D). Kyoto Encyclopedia of Genes and Genomes (KEGG) enrichment analysis showed the DEGs were enriched in various pathways, including adherens junction and focal adhesion (Figure 6E). Functional enrichment analysis of GO and KEGG using integrated fold change indicated a strong association between DEGs and cell adhesion (Figure 6F). Gene set enrichment analysis (GSEA) showed that genes related to cytokine receptor interaction and focal adhesion were significantly enriched after MARK4 knockdown compared with LPS stimulation (Figure 6G). The RT-qPCR method was used to validate the findings derived from RNA-seq. Three DEGs related to R-PMVEC inflammation and cell barrier, including GOLM1, APLNR, and FNDC5, were markedly elevated (Figure 6H). Six DEGs, including AEBP1, PIEZO1, FN1, MMP9, ECM1, and STAT3 were dramatically down-regulated after MARK4 knockdown. MARK4 knockdown reduced SELPLG gene expression compared to the LPS group, however the change was not statistically significant (Figure 6I). Among these DEGs, we identified PIEZO1, a gene highly linked to cell adhesion, which we selected as a key indication for further experimentation.

Overexpression of MARK4 in R-PMVEC Reversed the Protective Effect of Rhein

Firstly, we verified the mRNA expression level of MARK4 in R-PMVEC after LPS stimulation with different doses of rhein (Figure 7A). The results indicated that rhein could dose-dependently reduce the increase in MARK4 mRNA induced by LPS, and the protein expression of MARK4 and p-MAP4 (S1073) was consistent with this finding (Figure 7B). Figure 7C showed the molecular docking results between MARK4 and rhein. Subsequently, we over-expressed MARK4 in R-PMVEC (Supplementary Figure 2). The levels of inflammatory factors were consistent with previous results, showing that rhein could alleviate LPS-induced inflammation. However, inflammation levels rose again after overexpression of MARK4 (Figure 7D–F). The mRNA level of MARK4 correspondingly changed (Figure 7G). Overexpression of MARK4 reversed the therapeutic effect of rhein on the endothelial barrier and MT damage in R-PMVEC (Figure 7H), and similar results were observed in the IF assay of R-PMVEC (Figure 7I).

https://doi.org/10.2147/JIR.S505049

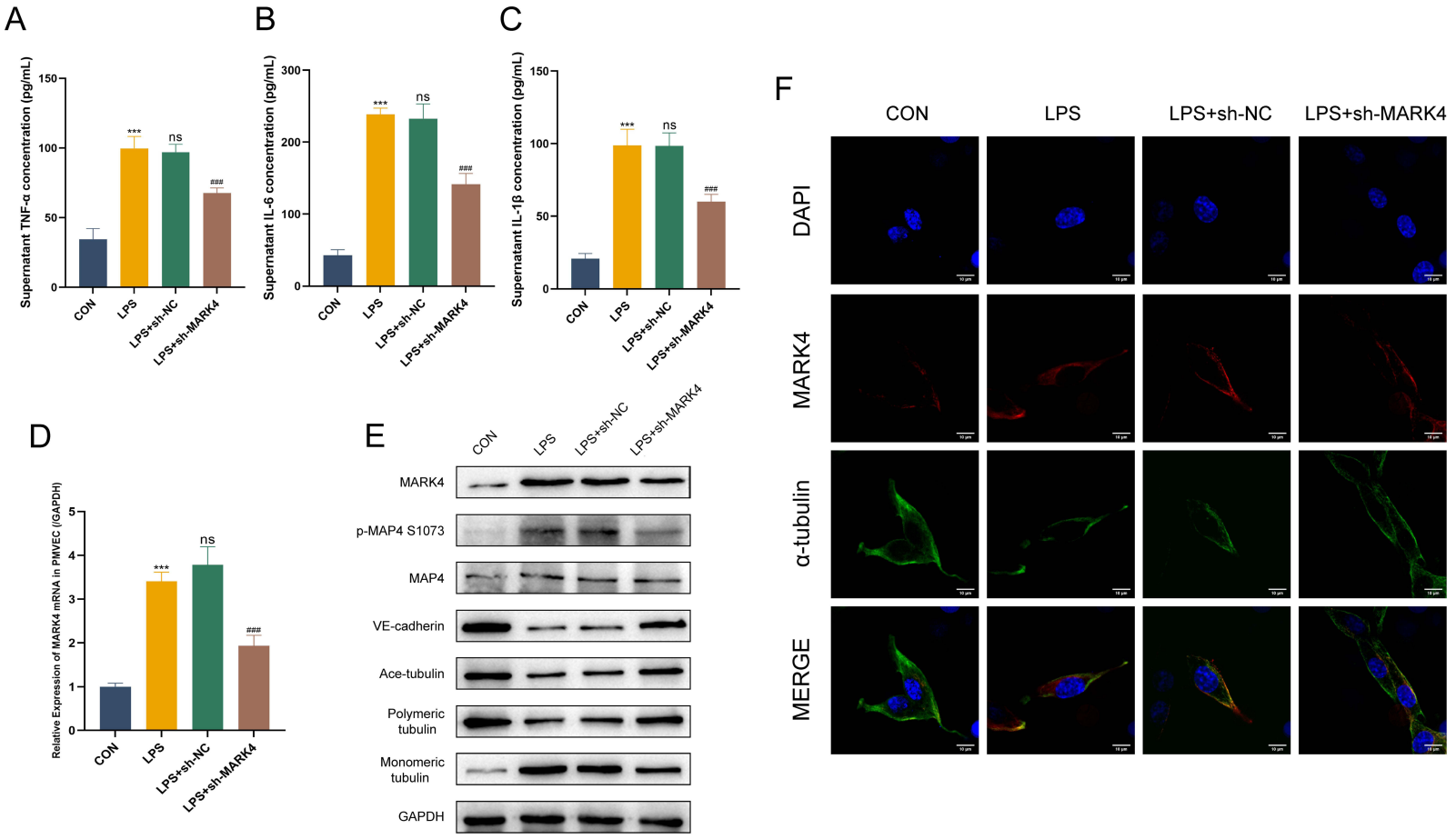

Figure 5 Protective effect of MARK4 knockdown on R-PMVEC injury induced by LPS. (**A–C**) Inflammatory factors TNF-α, IL-6, and IL-1β levels in R-PMVEC culture supernatant were detected by kits separately. (**D**) MARK4 mRNA relative expression in R-PMVEC was performed by Real-Time quantitative PCR. (**E**) Protein expression levels of MARK4, p-MAP4 (S1073), VE-cadherin, and MT-related proteins in R-PMVEC were performed by Western blot. (**F**) Immunofluorescence staining of MARK4 and MT in R-PMVEC. Data were representative images or expressed as mean ± standard deviation of each group at least three independent experiments. *** means P<0.001 compared with CON group; ns means no significance compared with LPS group; ### means P<0.001 compared with LPS group. scale bar: 10μm.

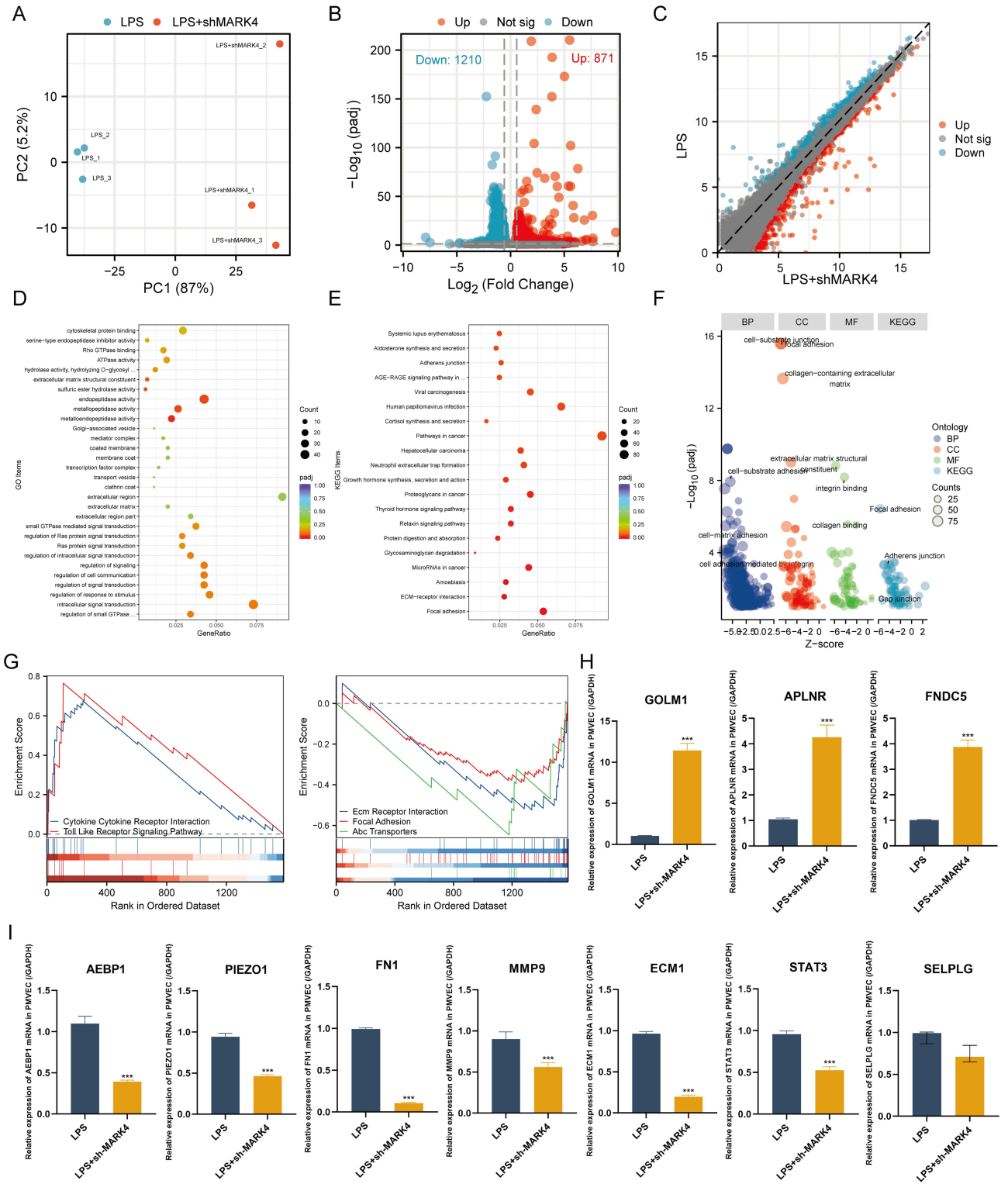

Figure 6 Results of RNA sequencing. (**A**) Principal component analysis for the transcriptome profiles. (**B** and **C**) Volcano plot of DEGs. GO (**D**) and KEGG (**E**) enrichment analysis of DEGs. (**F**) Functional enrichment analysis of GO and KEGG using integrated fold change. (**G**) GSEA showed that MARK4 could affect cytokine receptor interaction and focal adhesion. (**H** and **I**) Ten selected genes from DEGs mRNA relative expressions in R-PMVEC were performed using Real-Time quantitative PCR. | log2FoldChange| > 0.58 and padj < 0.05 were the cutoffs for DEGs. Data were representative images or expressed as mean ± SD or median with interquartile range of each group at least three independent experiments. *** means P<0.001 compared with LPS group.

https://doi.org/10.2147/JIR.S505049

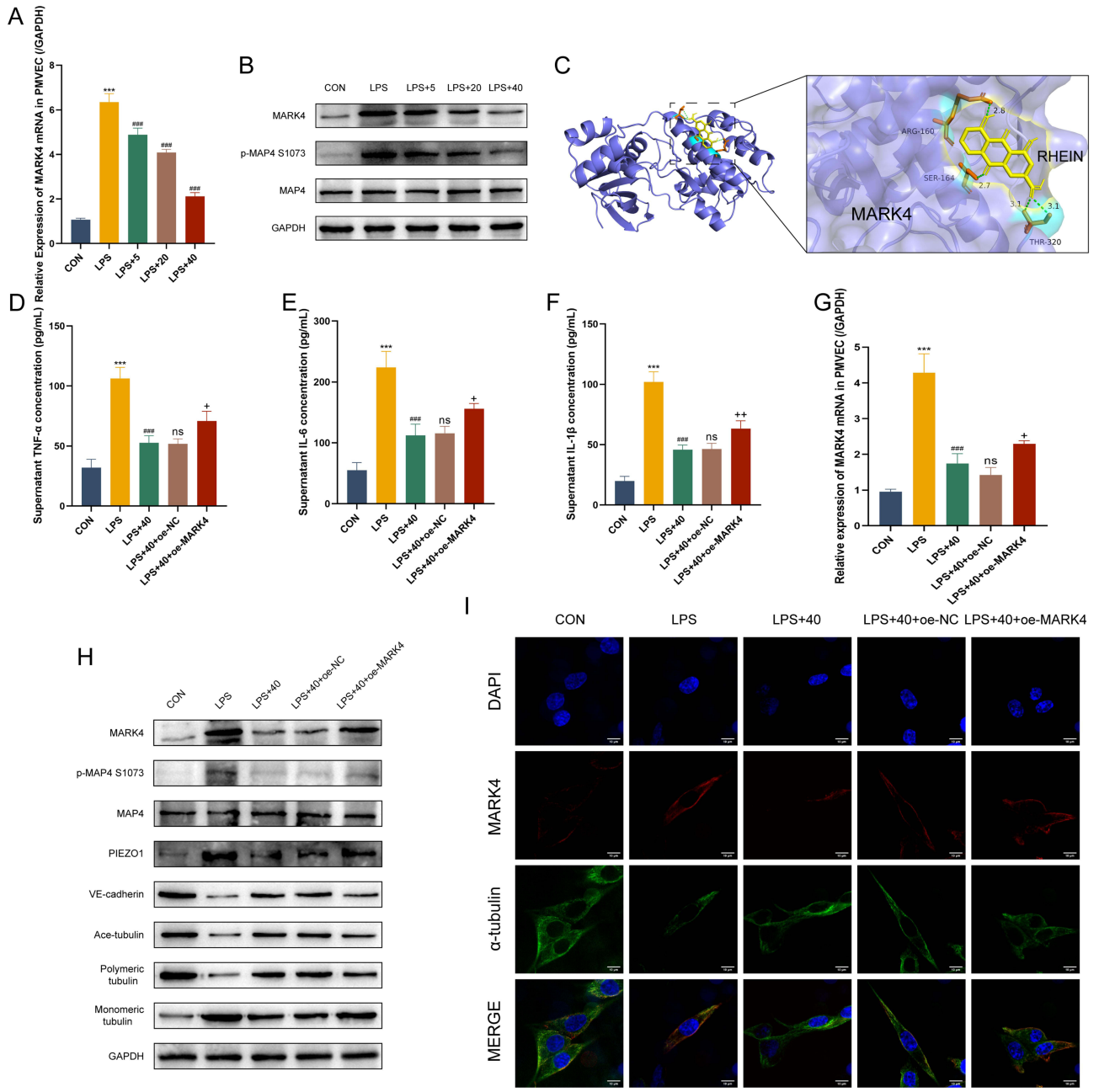

Figure 7 Overexpression of MARK4 in R-PMVEC reversed the protective effect of rhein. (**A**) MARK4 mRNA relative expression in R-PMVEC treated with different doses of rhein was performed by Real-Time quantitative PCR. (**B**) Protein expression levels of MARK4 and p-MAP4 (S1073) in R-PMVEC treated with different doses of rhein were performed by Western blot. (**C**) Molecular docking result of MARK4 and rhein. (**D**–**F**) Inflammatory factors TNF-α, IL-6, and IL-1β levels in R-PMVEC culture supernatant were detected by kits separately. (**G**) MARK4 mRNA relative expressions in R-PMVEC were performed by Real-Time quantitative PCR. (**H**) Protein expression levels of MARK4, p-MAP4 (S1073), PIEZO1, VE-cadherin, and MT-related proteins in R-PMVEC were performed by Western blot. (**I**) Immunofluorescence staining of MARK4 and MT in R-PMVEC. Data were representative images or expressed as mean ± SD of each group at least three independent experiments. *** means P<0.001 compared with CON group; ### means P<0.001 compared with LPS group; ns means no significance compared with LPS+40 group; + means P<0.05 compared with LPS+40+oe-NC group; ++ means P<0.01 compared with LPS+40 +oe-NC group. scale bar: 10μm.

Protective Effect of MARK4 Inhibitor or Rhein on Lung Injury in SAP Rats

PCR results showed that the mRNA levels of inflammatory factors in the SAP group were significantly higher than those in the SO group and decreased in the MARK inhibitor PCC0208017 treatment group (SAP+PCC) and the rhein treatment group (SAP+150) (Figure 8A–C). WB results indicated that the protein levels of p-MAP4 (S1073) and PIEZO1 increased in the SAP group, the endothelial barrier was damaged, and MT depolymerization occurred. These changes were

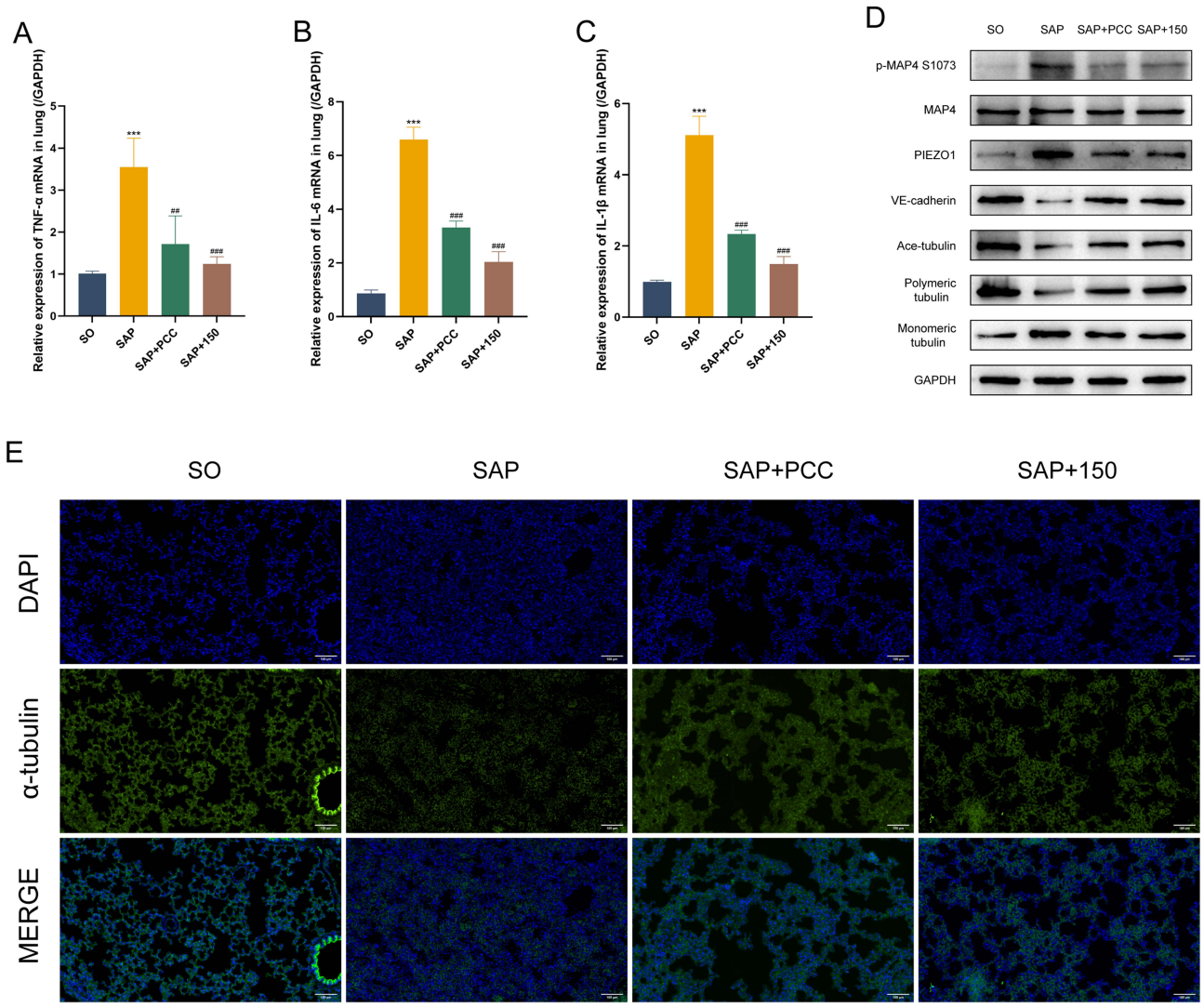

Figure 8 MARK4 inhibitor or rhein ameliorated lung injury in SAP-ALI rats. (**A**–**C**) TNF-α, IL-6, and IL-1β mRNA relative expressions in rat lungs were performed by Real-Time quantitative PCR. (**D**) Protein expression levels of p-MAP4 (S1073), PIEZO1, VE-cadherin, and MT-related proteins in rat lungs were performed by Western blot. (**E**) Immunofluorescence staining of MT in rat lungs. Data were representative images or expressed as mean ± SD of each group at least three independent experiments. *** means P<0.001 compared with CON group; ## means P<0.01 compared with SAP group; #### means P<0.001 compared with SAP group. scale bar: 100μm.

effectively reversed after applying PCC0208017 or rhein (Figure 8D). Consistently, lung tissue immunofluorescence also showed that apparent MT damage happened in the lungs of SAP group rats. After administration of the MARK4 inhibitor or rhein, the MT damage was significantly alleviated (Figure 8E).

Discussion

Under the stimulation of LPS, the levels of inflammatory factors in the cell culture supernatant significantly increased, while rhein could decrease the levels of these inflammatory factors in a concentration-dependent manner (5 μM, 20 μM, and 40 μM). The endothelial barrier and MT structure were damaged under inflammatory conditions, which was consistent with our previous research findings,[22] and rhein intervention could partially alleviate these changes. In addition, the results indicated that in vivo, rhein (50mg/kg, 100mg/kg, and 150mg/kg) significantly improved the severity of pancreatitis and pulmonary inflammatory responses, reduced the permeability of the pulmonary endothelial barrier, and mitigated the depolymerization of MT.

MARK4 is a serine/threonine kinase that modifies microtubule-associated proteins (MAPs, including tau, MAP2, and MAP4) through phosphorylation to alter microtubule structure.[23] Recent studies have also found that MARK4 can

https://doi.org/10.2147/JIR.S505049

participate in the regulation of inflammatory responses by modulating the formation of the NLRP3 inflammasome and activating the NF-κB signaling pathway.[24–26] However, there is currently no research on the role of MARK4 in SAP-ALI. MARK4 can induce the detachment of MAP4 from MT by phosphorylating the MT anchor site at the S1073 position of MAP4, leading to the depolymerization of the MT structure.[27,28] We proposed the hypothesis that during SAP-ALI, MARK4 might cause the depolymerization of MT in endothelial cells by phosphorylating the MAP4 S1073 site. We knocked down MARK4 in R-PMVEC, and the results showed a significant decrease in the phosphorylation level of MAP4 at the S1073 site, with a reduction in MT depolymerization. Additionally, the levels of inflammatory factors in the culture medium of R-PMVEC also decreased, suggesting that MARK4 may be involved in the inflammatory response induced by LPS. Subsequently, we conducted RNA sequencing on two groups of R-PMVEC samples (LPS vs LPS+sh-MARK4). Compared to stimulation with LPS alone, the knockdown of MARK4 resulted in changes in the expression of 2081 genes. Interestingly, Piezo-type mechanosensitive ion channel component 1 (PIEZO1) was also among DEGs. PIEZO1 is a mechanosensitive ion channel widely distributed in the lungs and involved in a variety of physiological processes.[29,30] PIEZO1 enhances the permeability of lung vascular endothelial cells by promoting the internalization and degradation of adherens junction protein VE-cadherin.[31] Under shear stress, PIEZO1 is activated, leading to an influx of extracellular Ca^{2+} and the activation of the protease calpain-2, which can hydrolyze the cytoskeleton.[32] Our findings indicate that MARK4 plays a role in regulating PIEZO1 expression in response to LPS stimulation.

Molecular docking was applied to simulate the binding of MARK4 with rhein, and the binding energy indicated a stable binding with strong affinity. The expression levels of MARK4 and MAP4 S1073 in cells decreased most significantly when treated with a higher concentration of rhein. To further validate this finding, we overexpressed MARK4 in R-PMVEC for a rescue experiment. The results demonstrated that overexpression of MARK4 could partially reverse the therapeutic effect of rhein, while the protein expression levels of MAP4 S1073 and PIEZO1 also increased again. Finally, a MARK4 inhibitor was used in vivo experiments to explore the potential role of MARK4 in SAP-ALI. PCC0208017 has been previously proven to possess potent inhibitory effects on the activity of MARK4.[33] The experimental results showed that, similar to rhein, the MARK4 inhibitor could also alleviate inflammatory response and depolymerization of MT in the rat lungs during SAP and affected the phosphorylation modification of MAP4 S1073 and the expression of PIEZO1.

Conclusion

Rhein may inhibit SAP-induced destruction and inflammation of pulmonary microvascular endothelial cells by inhibiting MARK4-mediated microtubule depolymerization. Our findings indicate that PIEZO1, a mechanically gated ion channel, may serve as a target gene for MARK4, suggesting a novel role for MARK4 beyond its established function in microtubule regulation. This study elucidates the pathogenesis of SAP-ALI and identifies potential therapeutic agents. Nonetheless, the current study is limited by its sample size and reliance on a single modelling method; future research should incorporate a larger sample to validate the therapeutic effects of rhein. The specific mechanism of endothelial cell damage mediated by the MAKR4-PIEZO1 axis we identified requires further investigation.

Abbreviations

AKP, alkaline phosphatase; ALI, acute lung injury; ALT, alanine aminotransferase; AP, acute pancreatitis; ARDS, acute respiratory distress syndrome; AST, aspartate aminotransferase; BALF, bronchoalveolar lavage fluid; BUN, blood urea nitrogen; CREA, creatinine; GO, gene ontology; LPS, lipopolysaccharide; MAP4, microtubule-associated protein 4; MARK4, microtubule affinity-regulating kinase 4; MODS, multiple organ dysfunction syndrome; MT, microtubule; PIEZO1, Piezo-type mechanosensitive ion channel component 1; PVDF, polyvinylidene fluoride; ROS, reactive oxygen species; SAP, severe acute pancreatitis; SAP-ALI, severe acute pancreatitis-associated acute lung injury; SIRS, systemic inflammatory response syndrome; TBST, Tris-buffered saline Tween 20.

Data Sharing Statement

The datasets used and/or analyzed during the present study are available from the corresponding author on reasonable request.

Acknowledgment

The authors would like to thank the reviewers, as well as BioRender.com for graphical abstract (Created in BioRender. Sun, z. (2025) https://BioRender.com/f65x070).

Funding

This study was supported by National Natural Science Foundation of China (NO. 82274311 and 82074158).

Disclosure

The authors declare no conflicts of interest in this work.

References

1. Forsmark CE, Vege SS, Wilcox CM. Acute Pancreatitis. *N Engl J Med*. 2016;375(20):1972–1981. doi:10.1056/NEJMra1505202
2. Landahl P, Ansari D, Andersson R. Severe acute pancreatitis: gut barrier failure, systemic inflammatory response, acute lung injury, and the role of the mesenteric lymph. *Surg Infect*. 2015;16(6):651–656. doi:10.1089/sur.2015.034
3. Zhu X, Duan F, Zhang Y, et al. Acadesine alleviates acute pancreatitis-related lung injury by mediating the barrier protective function of pulmonary microvascular endothelial cells. *Int Immunopharmacol*. 2022;111:109165. doi:10.1016/j.intimp.2022.109165
4. Jiang J, Ouyang H, Zhou Q, et al. LPS induces pulmonary microvascular endothelial cell barrier dysfunction by upregulating ceramide production. *Cell Signal*. 2022;92:110250. doi:10.1016/j.cellsig.2022.110250
5. Jiang J, Huang K, Xu S, Garcia J, Wang C, Cai H. Targeting NOX4 alleviates sepsis-induced acute lung injury via attenuation of redox-sensitive activation of CaMKII/ERK1/2/MLCK and endothelial cell barrier dysfunction. *Redox Biol*. 2020;36:101638. doi:10.1016/j.redox.2020.101638
6. Birukova AA, Birukov KG, Smurova K, et al. Novel role of microtubules in thrombin-induced endothelial barrier dysfunction. *FASEB J*. 2004;18 (15):1879–1890. doi:10.1096/fj.04-2328com
7. Kratzer E, Tian Y, Sarich N, et al. Oxidative stress contributes to lung injury and barrier dysfunction via microtubule destabilization. *Am J Respir Cell Mol Biol*. 2012;47(5):688–697. doi:10.1165/rcmb.2012-0161OC
8. Buglak DB, Bougaran P, Kulikauskas MR, et al. Nuclear SUN1 stabilizes endothelial cell junctions via microtubules to regulate blood vessel formation. *Elife*. 2023;12:e83652. doi:10.7554/eLife.83652
9. Xia J, Wang J, Liu F, et al. Red/NIR-I-fluorescence carbon dots based on rhein with active oxygen scavenging and colitis targeting for UC therapeutics. *Adv Healthc Mater*. 2024;13(19):e2304674. doi:10.1002/adhm.202304674
10. Huang J, Zhang H, Ma L, et al. Rhein and hesperidin nanoparticles remodel tumor immune microenvironment by reducing CAFs and CCL2 secreted by CAAs for efficient triple-negative breast cancer therapy. *Int Immunopharmacol*. 2024;141:113001. doi:10.1016/j.intimp.2024.113001
11. Chen Q, Guo H, Hu J, Zhao X. Rhein inhibits NF-κB signaling pathway to alleviate inflammatory response and oxidative stress of rats with chronic glomerulonephritis. *Appl Bionics Biomech*. 2022;2022:9671759. doi:10.1155/2022/9671759
12. Li RJ, Xu JJ, Zhang ZH, et al. Rhein ameliorates transverse aortic constriction-induced cardiac hypertrophy via regulating STAT3 and p38 MAPK signaling pathways. *Front Pharmacol*. 2022;13:940574. doi:10.3389/fphar.2022.940574
13. Zhou RN, Zhu ZW, Xu PY, et al. Rhein targets macrophage SIRT2 to promote adipose tissue thermogenesis in obesity in mice. *Commun Biol*. 2024;7(1):1003. doi:10.1038/s42003-024-06693-6
14. Qin X, Wang S, Huang J, et al. Rhein alleviates MPTP-induced Parkinson's disease by suppressing neuroinflammation via MAPK/IκB pathway. *Front Neurosci*. 2024;18:1396345. doi:10.3389/fnins.2024.1396345
15. Wang W, Wang Z, Yang X, et al. Rhein ameliorates septic lung injury and intervenes in macrophage metabolic reprogramming in the inflammatory state by Sirtuin 1. *Life Sci*. 2022;310:121115. doi:10.1016/j.lfs.2022.121115
16. Li X, Xiao C, Yuan J, Chen X, Li Q, Shen F. Rhein-attenuates LPS-induced acute lung injury via targeting NFATc1/Trem2 axis. *Inflamm Res*. 2023;72(6):1237–1255. doi:10.1007/s00011-023-01746-8
17. Shen C, Zhang Z, Xie T, et al. Rhein suppresses lung inflammatory injury induced by human respiratory syncytial virus through inhibiting NLRP3 inflammasome activation via NF-κB pathway in mice. *Front Pharmacol*. 2019;10:1600. doi:10.3389/fphar.2019.01600
18. Xu Q, Wang M, Guo H, et al. Emodin alleviates severe acute pancreatitis-associated acute lung injury by inhibiting the Cold-Inducible RNA-Binding Protein (CIRP)-Mediated Activation of the NLRP3/IL-1β/CXCL1 signaling. *Front Pharmacol*. 2021;12:655372. doi:10.3389/fphar.2021.655372
19. Mu S, Liu Y, Jiang J, et al. Unfractionated heparin ameliorates pulmonary microvascular endothelial barrier dysfunction via microtubule stabilization in acute lung injury. *Respir Res*. 2018;19(1):220. doi:10.1186/s12931-018-0925-6
20. Eberhardt J, Santos-Martins D, Tillack AF, Forli S. AutoDock Vina 1.2.0: new Docking Methods, expanded force field, and Python bindings. *J Chem Inf Model*. 2021;61(8):3891–3898. doi:10.1021/acs.jcim.1c00203
21. Trott O, Olson AJ. AutoDock Vina: improving the speed and accuracy of docking with a new scoring function, efficient optimization, and multithreading. *J Comput Chem*. 2010;31(2):455–461. doi:10.1002/jcc.21334
22. Cao Y, Li F, Sun Z, et al. Regulation of microtubule stability in pulmonary microvascular endothelial cells in rats with severe acute pancreatitis: Qingyi decoction is a potential CDK5 inhibitor. *J Inflamm Res*. 2024;17:2513–2530. doi:10.2147/JIR.S451755
23. Trinczek B, Brajenovic M, Ebneth A, Drewes G. MARK4 is a novel microtubule-associated proteins/microtubule affinity-regulating kinase that binds to the cellular microtubule network and to centrosomes. *J Biol Chem*. 2004;279(7):5915–5923. doi:10.1074/jbc.M304528200
24. Liu Z, Gan L, Chen Y, et al. Mark4 promotes oxidative stress and inflammation via binding to PPARγ and activating NF-κB pathway in mice adipocytes. *Sci Rep*. 2016;6:21382. doi:10.1038/srep21382

25. Luo Y, Huang Z, Mou T, et al. SET8 mitigates hepatic ischemia/reperfusion injury in mice by suppressing MARK4/NLRP3 inflammasome pathway. *Life Sci*. 2021;273:119286. doi:10.1016/j.lfs.2021.119286
26. Lei Y, Chen Y, Zhang S, Wang W, Zheng M, Zhang R. Qingzhuan dark tea Theabrownin alleviates hippocampal injury in HFD-induced obese mice through the MARK4/NLRP3 pathway. *Heliyon*. 2024;10(5):e26923. doi:10.1016/j.heliyon.2024.e26923
27. Zhang J, Li L, Zhang Q, et al. Phosphorylation of microtubule- associated Protein 4 promotes hypoxic endothelial cell migration and proliferation. *Front Pharmacol*. 2019;10:368. doi:10.3389/fphar.2019.00368
28. Yu X, Chen X, Amrute-Nayak M, et al. MARK4 controls ischaemic heart failure through microtubule detyrosination. *Nature*. 2021;594 (7864):560–565. doi:10.1038/s41586-021-03573-5
29. Zhong M, Komarova Y, Rehman J, Malik AB. Mechanosensing Piezo channels in tissue homeostasis including their role in lungs. *Pulm Circ*. 2018;8(2):2045894018767393. doi:10.1177/2045894018767393
30. Coste B, Mathur J, Schmidt M, et al. Piezo1 and Piezo2 are essential components of distinct mechanically activated cation channels. *Science*. 2010;330(6000):55–60. doi:10.1126/science.1193270
31. Friedrich EE, Hong Z, Xiong S, et al. Endothelial cell Piezo1 mediates pressure-induced lung vascular hyperpermeability via disruption of adherens junctions. *Proc Natl Acad Sci U S A*. 2019;116(26):12980–12985. doi:10.1073/pnas.1902165116
32. Li J, Hou B, Tumova S, et al. Piezo1 integration of vascular architecture with physiological force. *Nature*. 2014;515(7526):279–282. doi:10.1038/nature13701
33. Li F, Liu Z, Sun H, et al. PCC0208017, a novel small-molecule inhibitor of MARK3/MARK4, suppresses glioma progression in vitro and in vivo. *Acta Pharm Sin B*. 2020;10(2):289–300. doi:10.1016/j.apsb.2019.09.004